Itinerant memory dynamics and global bifurcations in chaotic neural networks

Hiroyuki Kitajima
Faculty of Engineering, Kagawa University, 2217-20 Hayashi, Takamatsu 761-0396, Japan

Tetsuya Yoshinaga
School of Health Sciences, The University of Tokushima, 3-18-15 Kuramoto, Tokushima 770-8509, Japan

Kazuyuki Aihara
Faculty of Engineering, The University of Tokyo, 7-3-1 Hongo, Bunkyo-ku, Tokyo 113-8656, Japan

Hiroshi Kawakami
Faculty of Engineering, The University of Tokushima, 2-1 Minamijosanjima, Tokushima 770-8506, Japan

(Received 7 February 2003; accepted 24 June 2003; published 22 August 2003)

We have considered itinerant memory dynamics in a chaotic neural network composed of four chaotic neurons with synaptic connections determined by two orthogonal stored patterns as a simple example of a chaotic itinerant phenomenon in dynamical associative memory. We have analyzed a mechanism of generating the itinerant memory dynamics with respect to intersection of a pair of α branches of periodic points and collapse of a periodic in-phase attracting set. The intersection of invariant sets is numerically verified by a novel method proposed in this paper. © *2003 American Institute of Physics.* [DOI: 10.1063/1.1601912]

Aihara *et al*. proposed a simple chaotic neuron model and an artificial neural network model composed of such chaotic neurons.[1–3] The models have been widely used for analysis of nonlinear neural dynamics with spatiotemporal chaos in associative memory networks,[1,4–6] combinatorial optimization networks,[7–10] and electronic implementation.[3,11,12] Among such studies we focus on the associative memory dynamics in this paper. Adachi and Aihara analyzed the dynamics of associative memory networks composed of chaotic neurons in detail and examined characteristics of the retrieval process.[4] However, the relation between dynamical association and chaotic itinerancy has not been clarified yet. In this paper we consider this relation from the viewpoint of nonlinear dynamical systems and illustrate that the generation of a chaotic itinerant phenomenon in a simple model of chaotic neural network is based on the intersection of a couple of unstable sets or α branches,[13] each of which is an invariant set associated with the characteristic multiplier of a periodic point outside the unit circle in the complex plane. Because the system is a noninvertible map,[14] the intersection of α branches is possible to occur and, in fact, is numerically verified by a novel method proposed in this paper.

I. INTRODUCTION

We analyze itinerant memory dynamics of a chaotic neural network[1,2] with respect to global bifurcations. A chaotic neural network is composed of chaotic neurons,[1,2] which were derived on the basis of the Caianiello neuronic equation[15] and the Nagumo–Sato neuronal model.[16]

Spatiotemporal dynamics of the chaotic neural network generates complex behavior with possible computational abilities. In particular, accumulating refractoriness inherent in the chaotic neurons makes it possible for the chaotic neural networks to escape from any fixed points except the quiescent state where all neurons are resting and keep itinerating in the state space. This unstable dynamics is useful for information processing such as dynamical association and combinatorial optimization.[1,3–8,17] These kinds of computational itinerant dynamics may be related to chaotic itinerancy.[18]

The purpose of this paper is to consider a mechanism of the generation of such chaotic itinerant memory dynamics observed when applied to associative memory, where the chaotic neural networks transit among stored states. Although chaotic itinerancy is typically observed in high-dimensional dynamical systems, it would be desirable, if possible, to treat a network model with a small size for considering the essential property.[5] We investigate a chaotic neural network composed of just four chaotic neurons with synaptic connections determined by two orthogonal stored patterns in this paper because we can calculate α branches of periodic points in detail for such a small-scale network.

II. CHAOTIC NEURAL NETWORK

We consider a network made up of four chaotic neurons[1–3] coupled by synaptic connection weights, which are determined according to orthogonal stored patterns $\mathcal{P}^1=(1,0,1,0)$ and $\mathcal{P}^2=(1,1,0,0)$.[5] The dynamics of the ith chaotic neuron is described as follows for $i=1,\ldots,4$ and $t=0,1,2,\ldots$:

$$o_i(t+1)=g\left(\sum_{j=1}^{4} W_{ij}\sum_{\tau=0}^{t}(k_f)^{\tau}o_j(t-\tau)-\alpha\sum_{\tau=0}^{t}(k_r)^{\tau}o_i(t-\tau)+A\right), \tag{1}$$

where $o_i(t+1)$ is the output between 0 and 1, W_{ij} is the synaptic weight from the jth chaotic neuron, k_f and k_r are decay parameters for the feedback inputs and the refractoriness, α is the refractory scaling parameter, and A is the bias including the threshold.[1–4] The nonlinear output function g of each neuron is assumed as follows:

$$g(u)=\frac{1}{1+\exp(-u/\varepsilon)}, \tag{2}$$

where ε is the steep parameter. The coupling coefficients are defined as follows:

$$W_{ij}=\sum_{k=1}^{2}\sigma_k\left(p_i^k-\frac{1}{2}\right)\left(p_j^k-\frac{1}{2}\right),\quad i,j=1,\ldots,4, \tag{3}$$

where p_i^k is the ith component of the kth pattern $\mathcal{P}^k$, and

$$\sigma_1=1-d,\quad \sigma_2=1+d. \tag{4}$$

Equation (1) can be simplified to the following simultaneous equations:[1–4]

$$\eta_i(t+1)=k_f\eta_i(t)+\sum_{j=1}^{4}W_{ij}g(\eta_j(t)+\zeta_j(t)),$$

$$\zeta_i(t+1)=k_r\zeta_i(t)-\alpha g(\eta_i(t)+\zeta_i(t))+a, \tag{5}$$

where η_i and ζ_i are internal states for the feedback inputs and the refractoriness, respectively, and

$$a=A(1-k_r).$$

Considering a small value of the parameter d in Eq. (4), we can treat a slightly asymmetric system with different weights among stored patterns. The connection matrix $W=\{W_{ij}\}_{i,j=1,\ldots,4}$ is given as follows:

$$W=\frac{1}{2}\begin{pmatrix} 1 & d & -d & -1 \\ d & 1 & -1 & -d \\ -d & -1 & 1 & d \\ -1 & -d & d & 1 \end{pmatrix}. \tag{6}$$

Assuming $|k_f|<1$, we have $\eta_1(t)+\eta_4(t)\to 0$ and $\eta_2(t)+\eta_3(t)\to 0$ as $t\to\infty$. Then the dynamics of Eq. (5) can be written as the following six-dimensional map:

$$T_2:R^6\to R^6$$

$$\begin{pmatrix} x\\ y\\ z\\ u\\ v\\ w \end{pmatrix}\mapsto\begin{pmatrix} k_rx-\alpha g(x+z)+a \\ k_ry-\alpha g(y-z)+a \\ k_fz+\frac{1}{2}(g(x+z)-g(y-z))+\frac{1}{2}d(g(u+w)-g(v-w)) \\ k_ru-\alpha g(u+w)+a \\ k_rv-\alpha g(v-w)+a \\ k_fw+\frac{1}{2}(g(u+w)-g(v-w))+\frac{1}{2}d(g(x+z)-g(y-z)) \end{pmatrix}. \tag{7}$$

Note that Eq. (7) with $d=0$ is reduced to two independent subsystems, each of which has the same dynamics. For example, the subsystem of (x,y,z) is written as follows:

$$T_1:R^3\to R^3$$

$$\begin{pmatrix} x\\ y\\ z \end{pmatrix}\mapsto\begin{pmatrix} k_rx-\alpha g(x+z)+a \\ k_ry-\alpha g(y-z)+a \\ k_fz+\frac{1}{2}(g(x+z)-g(y-z)) \end{pmatrix}. \tag{8}$$

A. Property of T_2

We are interested in the system T_2 with $|d|\ll 1$. In this case, T_2 is a perturbation system from a direct sum of two identical subsystems, each of which is described by T_1. The direct sum of invariant sets appearing in T_1 comes to be invariant sets in the direct sum system, so we have combinations of invariant sets. The stability of these invariant sets depends on the stability of the complementary subspace of a subspace in T_1. Therefore both the symmetry of T_1 itself and the symmetry of T_2 caused by the connection should be considered.

Here we note symmetric properties of T_2. By defining the following two transformations:

$$P_2:R^6\to R^6$$

$$\begin{pmatrix} x\\ y\\ z\\ u\\ v\\ w \end{pmatrix}\mapsto\begin{pmatrix} 0&1&0&0&0&0\\ 1&0&0&0&0&0\\ 0&0&-1&0&0&0\\ 0&0&0&0&1&0\\ 0&0&0&1&0&0\\ 0&0&0&0&0&-1 \end{pmatrix}\begin{pmatrix} x\\ y\\ z\\ u\\ v\\ w \end{pmatrix}, \tag{9}$$

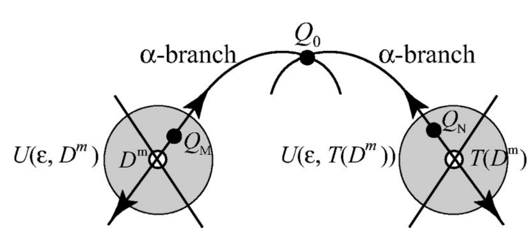

FIG. 1. Schematic diagram for intersection of α branches.

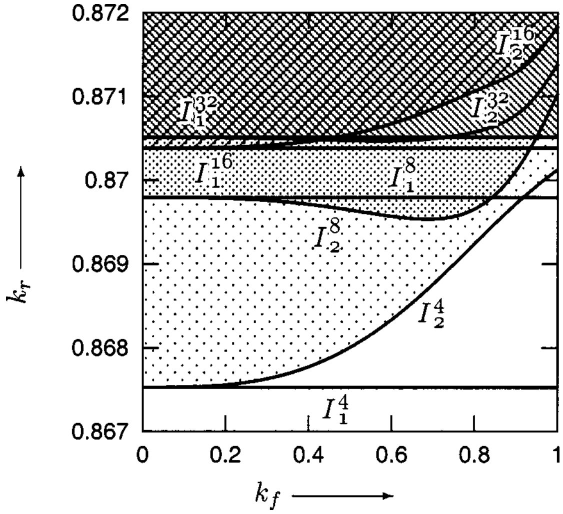

FIG. 2. Bifurcations of periodic points in T_1. The symbols I_1^m and I_2^m denote period-doubling bifurcations of m-periodic points.

and

$$Q_2: R^6 \to R^6$$

$$\begin{pmatrix} x \\ y \\ z \\ u \\ v \\ w \end{pmatrix} \mapsto \begin{pmatrix} 0 & 0 & 0 & 1 & 0 & 0 \\ 0 & 0 & 0 & 0 & 1 & 0 \\ 0 & 0 & 0 & 0 & 0 & 1 \\ 1 & 0 & 0 & 0 & 0 & 0 \\ 0 & 1 & 0 & 0 & 0 & 0 \\ 0 & 0 & 1 & 0 & 0 & 0 \end{pmatrix} \begin{pmatrix} x \\ y \\ z \\ u \\ v \\ w \end{pmatrix}, \tag{10}$$

a set of matrices representing transformations, each of which and T_2 are commutative, is obtained as follows:

$$G_2 = \{I, P_2, Q_2, P_2Q_2\}, \tag{11}$$

where I denotes the identity transformation. The above-given set forms a group with respect to the product of matrices. There exist invariant sets, including chaotic attractors as well as periodic points, which behave in the invariant subspace with respect to the transformation in Eq. (11). For example, an invariant set with respect to P_2 is called a P_2-invariant set.

B. Property of T_1

The behavior of a Q_2-invariant set is governed by the dynamics in Eq. (8). We note that Eq. (8) satisfies the symmetric property $P_1 \circ T_1 = T_1 \circ P_1$ where

$$P_1: R^3 \to R^3$$

$$\begin{pmatrix} x \\ y \\ z \end{pmatrix} \mapsto P_1 \begin{pmatrix} x \\ y \\ z \end{pmatrix} = \begin{pmatrix} 0 & 1 & 0 \\ 1 & 0 & 0 \\ 0 & 0 & -1 \end{pmatrix} \begin{pmatrix} x \\ y \\ z \end{pmatrix}. \tag{12}$$

This implies that the set of transformations $G_1 = \{I, P_1\}$ is an Abelian group. In other words, the map T_1 is G_1-equivariant. Therefore the line L_1 with $x = y$ and $z = 0$ is invariant with respect to the transformation P_1.

III. METHOD OF ANALYSIS

Before showing our results of analysis, we introduce the method for calculating an intersection of the α branch or unstable manifold and local bifurcations of periodic points.

Consider, in general, the following noninvertible map T:

$$T: R^n \to R^n; \quad u \mapsto T(u). \tag{13}$$

The point u^* satisfying

$$u^* - T^m(u^*) = 0 \tag{14}$$

becomes a fixed $(m=1)$ or an m-periodic $(m>1)$ point of T. Let $u^* \in R^n$ be a periodic point of T, then the characteristic equation of the periodic point u^* with respect to the characteristic multiplier μ is defined as follows:

$$\det(\mu I - DT^m(u^*)) = 0, \tag{15}$$

where I is the $n \times n$ identity matrix, and DT^m denotes the derivative of T^m. The point u^* is said to be hyperbolic, if all

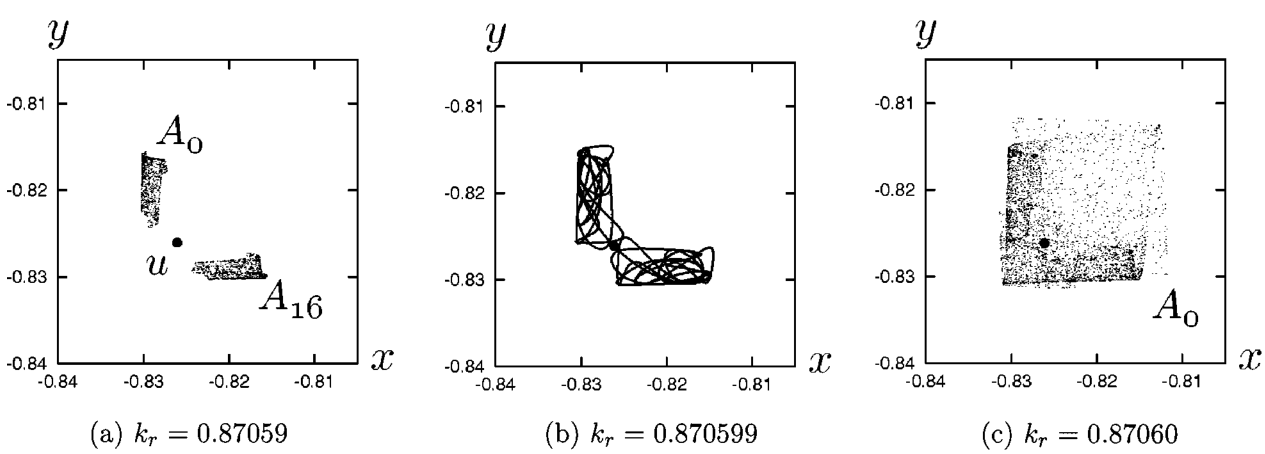

FIG. 3. (a) $k_r = 0.870\,59$. (b) $k_r = 0.870\,599$. (c) $k_r = 0.870\,60$. Phase portrait of iterated points, in (a) and (c), and a couple of P_1-symmetric α branches contacted each other, in (b), by T_1 with $k_f = 0.3$. Symbols A_i $(i = 0,16)$ and u denote parts of periodic attracting sets and periodic points, respectively.

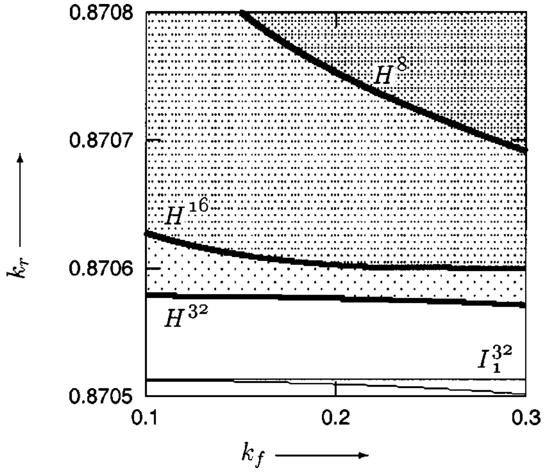

FIG. 4. Parameter regions for intersections of α branches of periodic points in T_1.

the absolute values of the eigenvalues of DT^m are different from unity. The symbol ${}_kD^m$ (respectively, ${}_kI^m$) denotes a hyperbolic periodic point, where D (respectively, I) indicates a periodic point with an even (respectively, odd) number of characteristic multipliers on the real axis $(-\infty,-1)$, k indicates the number of characteristic multipliers outside the unit circle in the complex plane, and m indicates an m-periodic point. An attracting set[19] is called periodic with period m if it is made up of m disjoint sets $A=\cup_{i=0}^{m-1}A_i$, where each A_i is an attracting set of the map T^m.

A. Calculating intersection of α branches

In this section we propose a novel method for generally calculating intersection of α branches of an m-periodic point for a three-dimensional system in Eq. (13) with $n=3$.

Let us consider the intersection of α branches of D^m and $T(D^m)$, where D^m is an unstable m-periodic point satisfying

$$T^m(D^m)=D^m, \quad T^k(D^m)\neq D^m \quad \text{for } 1\leqslant k<m. \tag{16}$$

Note that for the occurrence of intersection of α branches, the map T should be noninvertible. We take ϵ neighborhoods $U(\epsilon,D^m)$ and $U(\epsilon,T(D^m))$, i.e., $U(\epsilon,D^m)=\{x\in R^3: |x-D^m|<\epsilon\}$, as shown in Fig. 1. Then there exist positive integers M and N such that

$$Q_0=T^M(Q_M), \quad Q_M\in U(\epsilon,D^m), \tag{17}$$

$$Q_0=T^N(Q_N), \quad Q_N\in U(\epsilon,T(D^m)). \tag{18}$$

Substituting Eq. (18) into Eq. (17), we obtain

$$T^M(Q_M)-T^N(Q_N)=0. \tag{19}$$

We set ϵ to be sufficiently small, so that inside $U(\epsilon,D^m)$ the α branch of D^m can be well approximated by the unstable eigenspaces E^u of the Jacobi matrix of T at D^m.[20–22] The condition such that the points Q_M and Q_N belong to α branches is written as

$$(Q_M-D^m)\times e_1=O, \tag{20}$$

$$(Q_N-T(D^m))\times e_2=O, \tag{21}$$

where O is the zero vector, and e_1 and e_2 are eigenvectors associated with a characteristic multiplier μ_α $(|\mu_\alpha|>1)$, respectively, satisfying

$$(\mu_\alpha I-DT(D^m))e_1=O, \quad (\mu_\alpha I-DT^2(D^m))e_2=O. \tag{22}$$

If α branches intersect each other at the point Q_0, then Eq. (19) is independent of Eqs. (20) and (21). Therefore we can determine the variables $(D^m,Q_M,Q_N,\lambda)\in R^{10}$ for the set of Eqs. (16), (19), (20), and (21) by Newton's method, where λ is one of parameters included in the map T. Then the Jacobi matrix of Newton's method must be calculated. For this purpose, we repeatedly use the variational equations with respect to the initial condition and the system parameter, respectively, given by

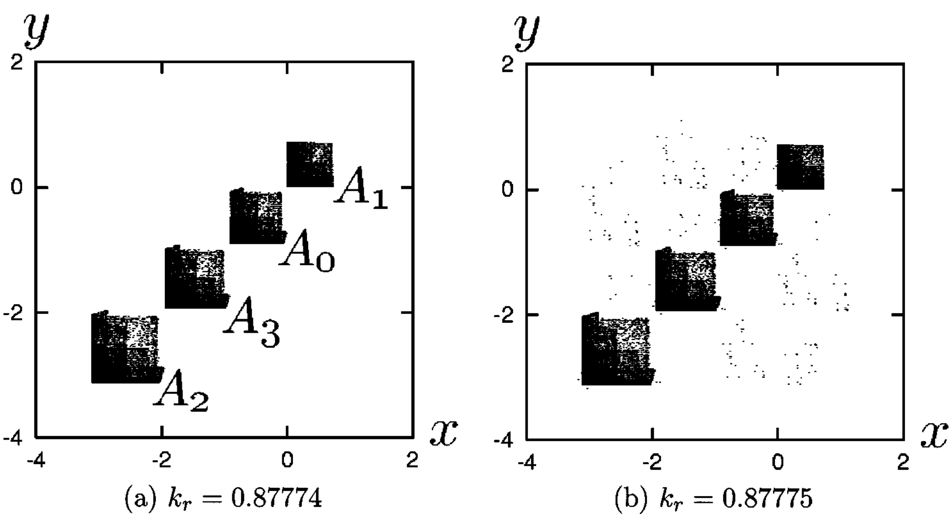

FIG. 5. (a) $k_r=0.87774$. (b) $k_r=0.87775$. Collapse of in-phase-locked chaos in T_1 with $k_f=0.3$.

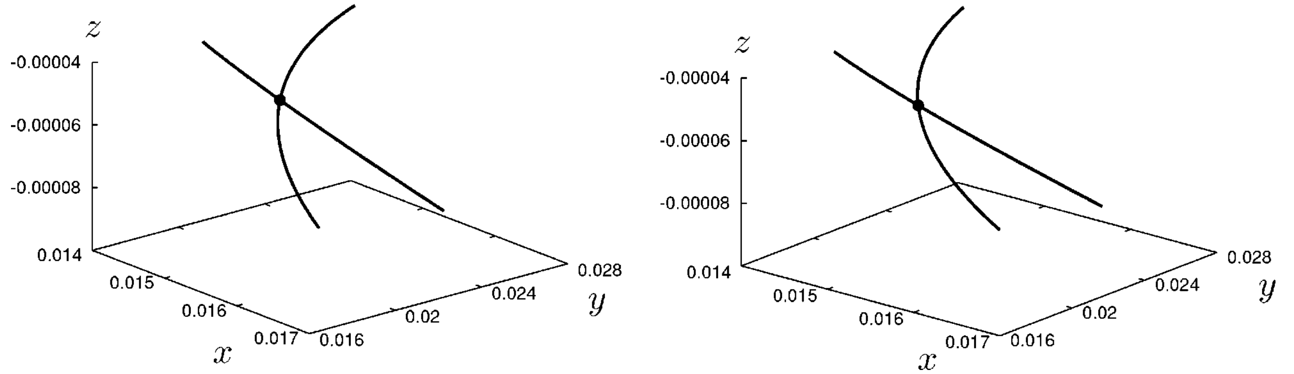

FIG. 6. A perspective figure of the three-dimensional phase portrait for the intersecting point Q_0 (circled point) and a couple of α-branches $W^+({}_2D^4)$ and $W^+(T_1({}_2D^4))$ with respect to the four-periodic points ${}_2D^4$ and $T_1({}_2D^4)$, respectively. Unrelated branches are omitted.

$$\frac{\partial \varphi}{\partial u}(t,u,\lambda)=\frac{\partial T}{\partial x}\frac{\partial \varphi}{\partial u}(t-1,u,\lambda), \quad \text{with } \frac{\partial \varphi}{\partial u}(0,u,\lambda)=I,$$

$$\frac{\partial \varphi}{\partial \lambda}(t,u,\lambda)=\frac{\partial T}{\partial x}\frac{\partial \varphi}{\partial \lambda}(t-1,u,\lambda)+\frac{\partial T}{\partial \lambda},$$

$$\text{with } \frac{\partial \varphi}{\partial \lambda}(0,u,\lambda)=O,$$

where $\varphi(t,u,\lambda)$ is a solution of Eq. (13) with $\varphi(0,u,\lambda)=u$.[23]

B. Calculating local bifurcation

A local bifurcation occurs when the topological type of a periodic point is changed by the variation of a system parameter. The generic bifurcations of the periodic point are known as codimension-one bifurcations: namely, tangent, period-doubling, and the Neimark–Sacker bifurcations. These bifurcations are observed when the hyperbolicity is destroyed, which corresponds to the critical distribution of the characteristic multiplier μ such that $\mu=+1$ for the tangent bifurcation, $\mu=-1$ for the period-doubling bifurcation, and $\mu=e^{j\theta}$ for the Neimark–Sacker bifurcation, where $j=\sqrt{-1}$ and $\theta\in R$. To calculate local bifurcations, we use the method proposed in Ref. 23. Namely the fixed (or periodic) point equation of Eq. (14) and the bifurcation condition of Eq. (15) are simultaneously solved by Newton's method.

In the bifurcation diagrams of Sec. IV, period-doubling bifurcation sets of an m-periodic point are indicated by curves with symbols I_ℓ^m, where ℓ is the index number to distinguish bifurcations of the same type.

IV. RESULTS OF ANALYSIS

In Eq. (7), the system parameters except k_f and k_r are fixed as follows:

$$\alpha=4, \quad a=0.8, \quad \varepsilon=0.015. \tag{23}$$

The parameter setting is based on lots of theoretical and numerical results[1–4,7,8] not only on periodic points but also on chaotic attractors in chaotic neural networks, producing rich dynamics with memory retrieving and searching processes.

The motion of a periodic point that is invariant with respect to the transformation Q_2 is restricted to the dynamics of T_1. Therefore, we first focus periodic points related to the occurrence of chaotic itinerancy in T_1, and consider both local and global bifurcations of the periodic points. Then, we investigate the system T_2 perturbed from the direct sum of two identical T_1's.

A. Chaotic itinerancy in T_1

We first explain a mechanism of the generation of chaotic itinerancy observed in the subsystem T_1 by extending the former result[5] with calculating intersection of α branches.

1. Generation of in-phase-locked chaos

A bifurcation diagram for period-doubling bifurcations of periodic points located on the invariant set L_1 is shown in Fig. 2. Each curve I_1^m with $m=2^k$ for $k=2,3,4,5$ shows a period-doubling bifurcation set of an m-periodic point, whose eigenvector associated with the characteristic multiplier -1 has the same direction as the line L_1. Because this phenomenon is equivalent to the period-doubling bifurcation appearing in a one-dimensional map: $R\to R$; $x\mapsto k_r x-\alpha g(x)+a$, the bifurcation curve is independent of the parameter k_f, as shown in Fig. 2. A $2m$-periodic point bifurcates to an orthogonal direction with respect to the line L_1, by passing through the period-doubling bifurcation curve I_2^m with increasing the parameter value of k_r. The areas in which unstable periodic points ${}_2D^m$ with $m=4,8,16$ and 32 exist are shown by shading loosely-

TABLE I. An example of the values for the intersection of α branches.

$\lambda=k_r=0.877\,799\,997\,8$
${}_2D^4=(-0.848\,864\,818\,7,-0.848\,864\,818\,7,0)$
$T_1({}_2D^4)=(0.054\,866\,464\,0,0.054\,866\,464\,0,0)$
$M=80,\ N=60$
$Q_M=(-0.841\,063\,167\,2,-0.856\,666\,470\,1,-0.000\,263\,068\,2)$
$Q_N=(0.054\,865\,723\,7,0.054\,867\,204\,5,0.000\,000\,008\,5)$
$T_1^M(Q_M)=(0.014\,755\,074\,1,0.022\,178\,454\,0,-0.000\,056\,812\,1)$
$T_1^N(Q_N)=(0.014\,755\,075\,0,0.022\,178\,450\,3,-0.000\,056\,812\,1)$

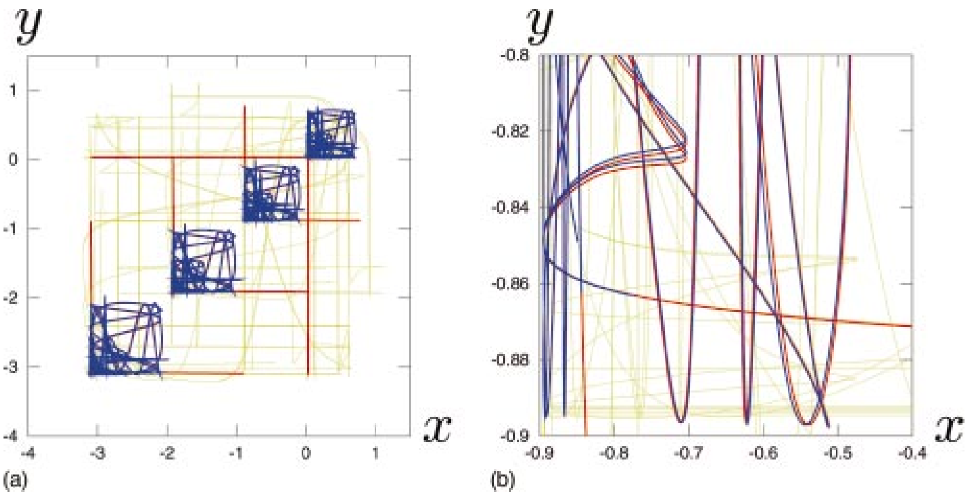

FIG. 7. (Color) The (x,y)-projection of α-branches $W^{+}(T_1^n(u))$, $n=0,1,2,3$, with respect to four-periodic point u of T_1 at each of the k_r values 0.877 74 (blue), 0.877 75 (red), and 0.877 77 (yellow). (b) A partially enlarged diagram of (a).

packed dots, tightly packed dots, lines from top right to bottom left, and lines from top left to bottom right, respectively.

We note that a mechanism of the generation of almost in-phase-locked chaos is related to the set of an α-branch $W^{+}({}_2D^m)$ of the m-periodic point associated with the eigenvector $(\pm p, \mp p, q)$, where p and q are nonzero constants. Figures 3(a) and 3(c) show an example of the transition before and after generation of an almost in-phase-locked chaos including a subset of the invariant set L_1. A part of T_1^{32}-invariant periodic attracting sets A_i $(i=0,\ldots,31)$ is shown in Fig. 3(a). The disjoint attracting set A_i satisfies $P_1(A_i)=A_j$, $j=i+16$ $(i=0,\ldots,15)$, so a couple of the sets A_i and $P_1(A_i)$ is T_1^{16}-invariant. By varying the param-

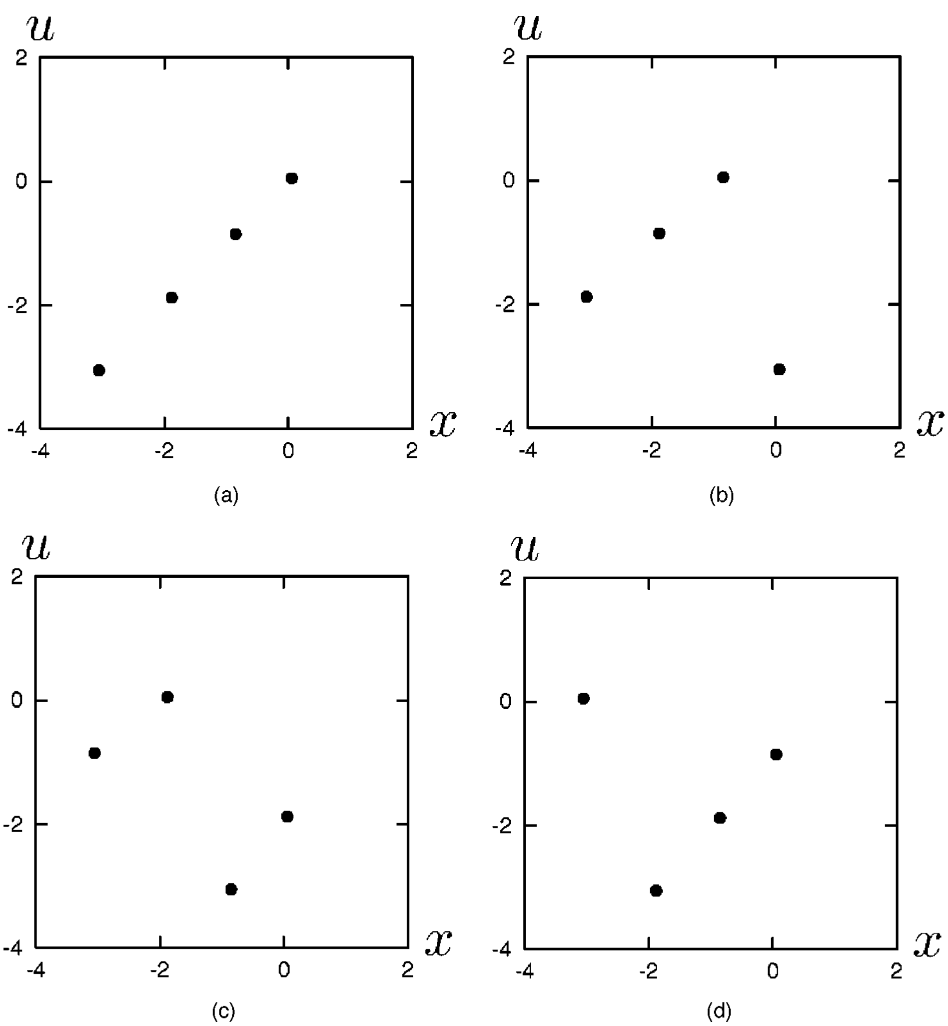

FIG. 8. Phase portraits of four periodic points with type ${}_4D^4$ in T_2 with $k_r=0.877\,70$.

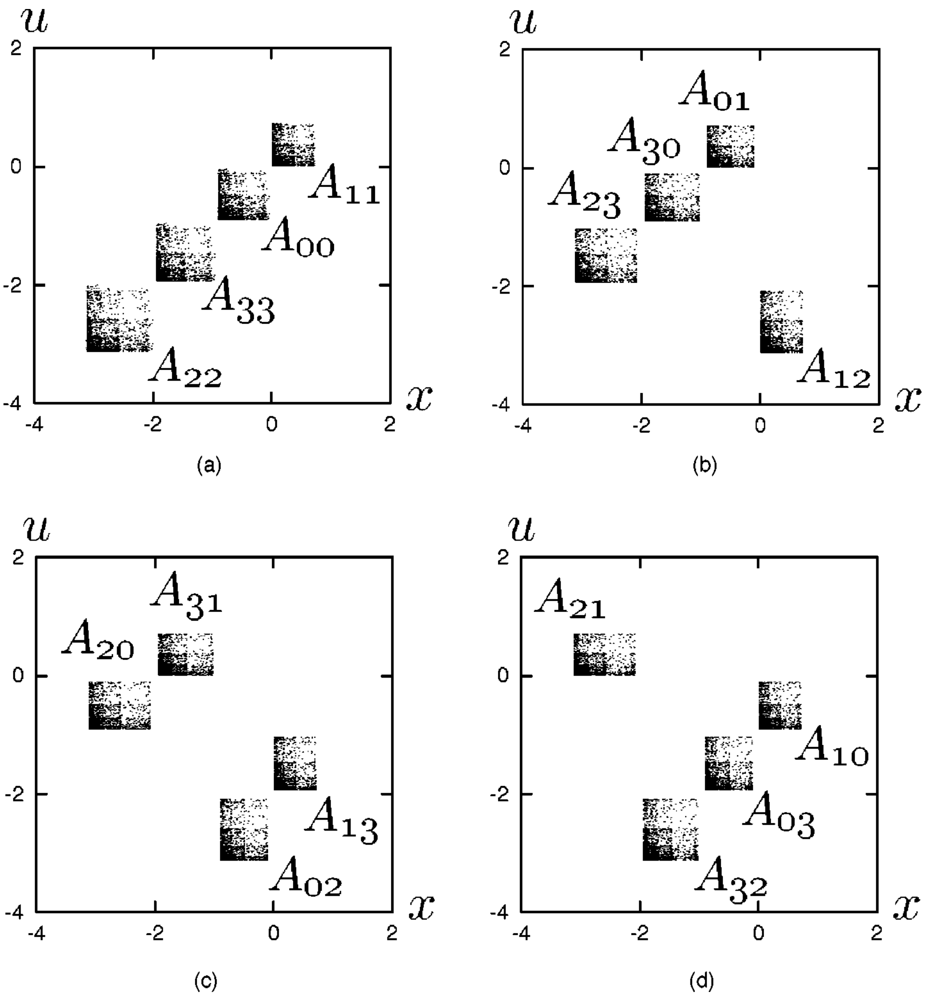

FIG. 9. Phase portraits of four types of four-periodic chaotic attracting sets in T_2 with $k_r = 0.877\,70$.

eter value of k_r from 0.870 59 to 0.870 60, A_i and $P_1(A_i)$ overlap as shown in Fig. 3(c). The generated attracting set is 16-periodic. This phenomenon is caused by the intersection of α-branches $W^+({}_2D^{16})$ and $P_1(W^+({}_2D^{16}))$ as illustrated in Fig. 3(b). By using the property that the intersecting point is located in L_1, the parameter set can be numerically obtained by a modified method presented in Ref. 24. The curve H^m $(m = 8,16,32)$ in Fig. 4 denotes the parameter set in

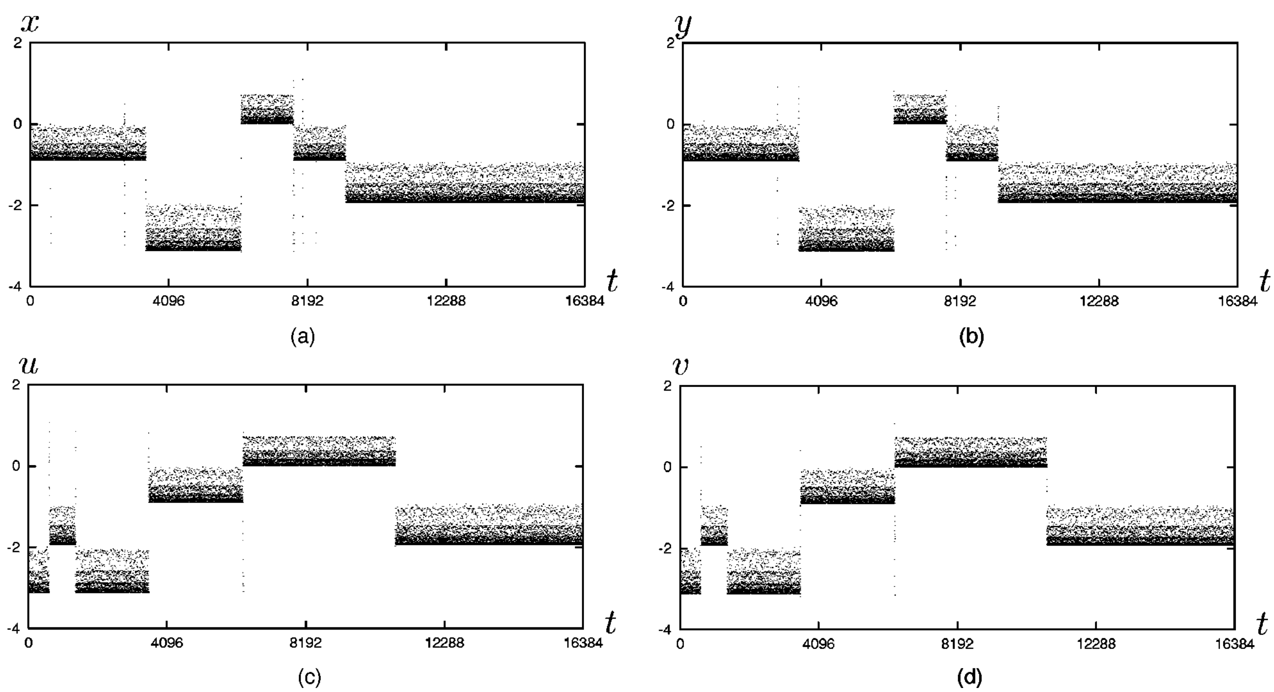

FIG. 10. Time series for iterated points of T_2^4 with $k_r = 0.877\,75$.

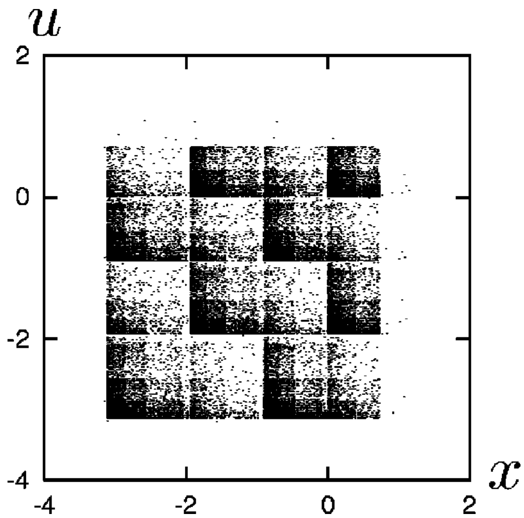

FIG. 11. Phase portrait of the attractor showing chaotic itinerancy observed in T_2 with $k_r = 0.877\ 75$.

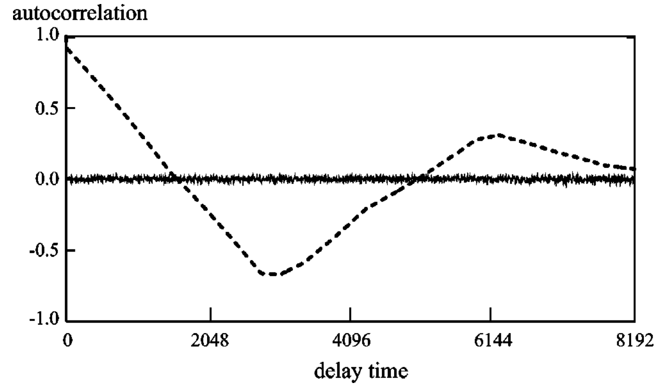

FIG. 13. Autocorrelation function for the chaotic attracting sets in T_2 with $k_r = 0.877\ 70$ (solid line) and $k_r = 0.877\ 75$ (dashed line).

which the condition $W^{+}({}_2D^m) \cap P_1(W^{+}({}_2D^m)) \neq \phi$ is satisfied. Therefore we see that an m-periodic attracting set exists in the shaded portions of tightly-packed dots, diagonally-packed dots and straight packed dots or regions surrounded by the curves H^m with $m = 8$, 16, and 32, respectively.

2. Collapse of in-phase-locked chaos

Figures 5(a) and 5(b) show that, by a slight change of the value of k_r, the four disjoint attracting sets come to be connected to each other and then iterated points of T_1 move without a locking property. Namely, the in-phase-locked chaos as a four-periodic attracting set collapses due to the occurrence of the following condition:

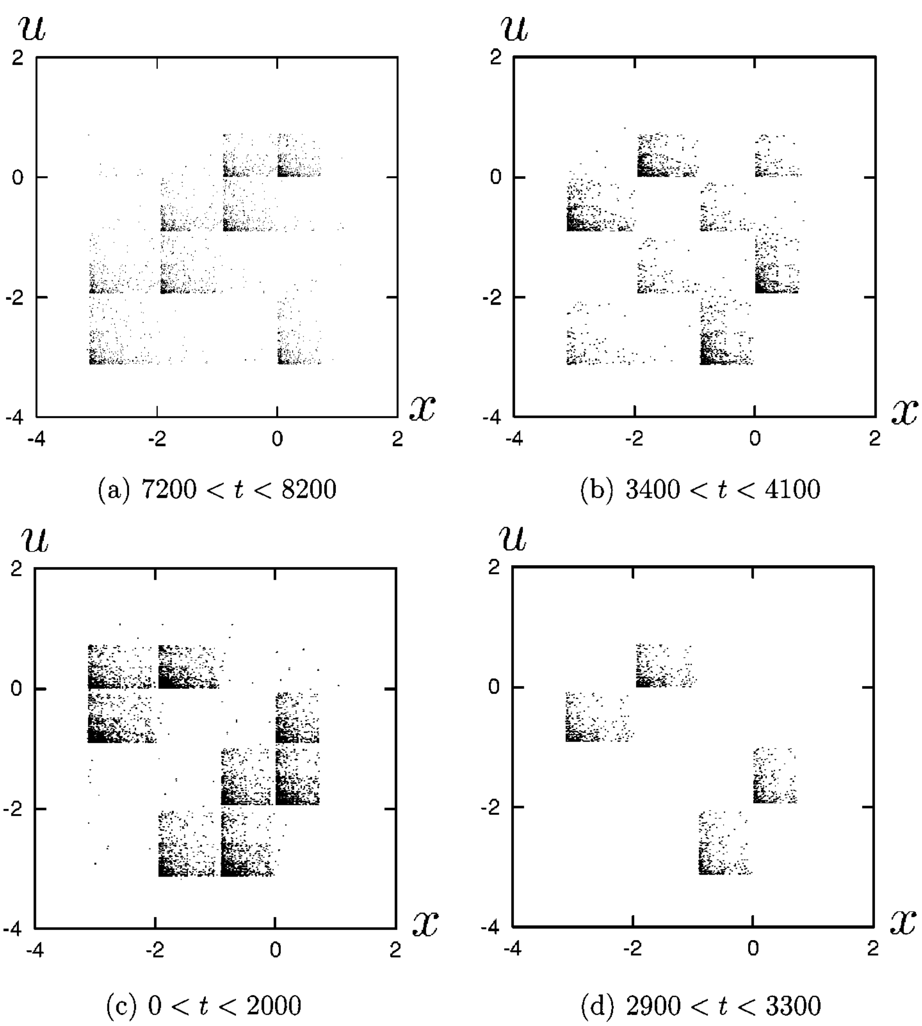

FIG. 12. Phase portrait of the same attractor as shown in Fig. 11 in short-term intervals.

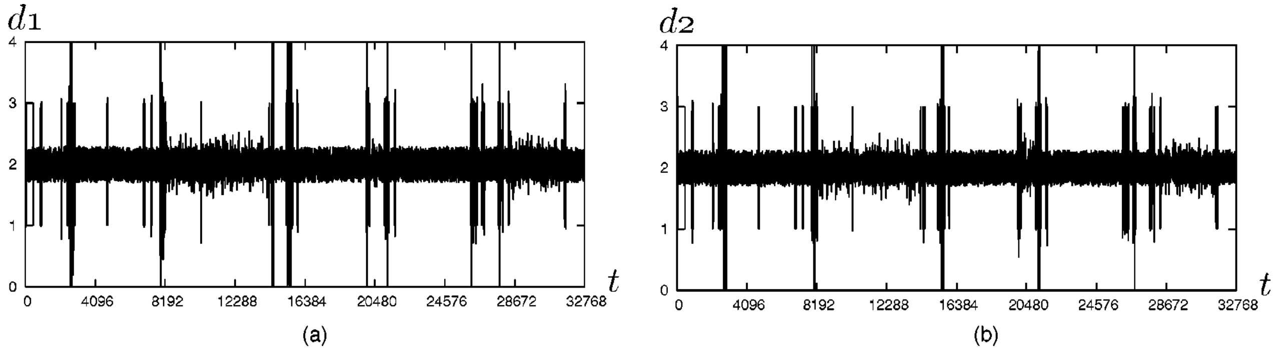

FIG. 14. Distance between the output patterns of T_2 with $k_r = 0.8778$ and the stored patterns (a) $\mathcal{P}^1$ and (b) $\mathcal{P}^2$.

$$W^+({}_2D^4) \cap W^+(T_1^n({}_2D^4)) \neq \phi, \quad \text{for } \exists n \in [1,2,3]. \tag{24}$$

In fact, we can confirm the intersection of α branches as shown in Fig. 6. The intersecting point in the state space can be calculated by the method presented in Sec. III A. The concrete values of variables obtained after convergence within predefined accuracy are shown in Table I.

A mechanism of the merging of T_1^4-invariant periodic attracting sets is illustrated as follows. Figure 7 shows α-branches $W^+(T_1^n(u))$, $n = 0,1,2,3$, with respect to four-periodic points u of T_1 with different parameter values. To compare the abrupt change of α branches by the parameter variation of the order of 10^{-5}, three different α branches, at $k_r = 0.877\,74$ (blue), 0.877 75 (red), and 0.877 77 (yellow), are overlapped in the figure. After merging of periodic attracting sets, the α branches with red and yellow colored curves extend to outside the area where the in-phase-locked chaos exists before merging. Parts of branches that are the most different from each other are shown in Fig. 7(b).

B. Itinerant memory dynamics in T_2

Next, let us consider T_2 with variation of the parameter value of k_r for the fixed parameter values $d = 0.01$ and $k_f = 0.3$.

The direct sum system of two identical subsystems has four kinds of four-periodic points as direct sum sets of the in-phase-locked four-periodic point ${}_2D^4$ of T_1. Because the direct sum of the periodic point ${}_2D^4$ are P_2-invariant in the six-dimensional state space, they also exist in T_2 with any value of d. Figure 8 shows phase portraits of the periodic points ${}_4D^4$ in T_2 with $k_r = 0.877\,70$. Four kinds of four-periodic points are P_2-invariant or satisfy $x = y$, $u = v$, and $z = w = 0$. Additionally, the periodic point shown in Fig. 8(a) is Q_2-invariant or satisfies $x = u$. In the following, we show a mechanism of the generation of chaotic itinerancy observed in T_2 with variation of the parameter value of k_r.

1. Coexistence of P_2-invariant and in-phase-locked periodic attracting sets

We show four types of four-periodic chaotic attracting sets at $k_r = 0.877\,70$ in Fig. 9. The set labeled by the symbol A_{ij} in the figure satisfies

$$A_{i+1,j+1} = T_2(A_{ij}), \tag{25}$$

where the suffix is an integer mod 4. Each attracting set is P_2-invariant and has the following properties.

(1) The attracting set shown in Fig. 9(a) is Q_2-invariant. We call it an in-phase-locked periodic attracting set, because its motion is restricted to an invariant subspace around $x = y = u = v$ and $z = w = 0$.
(2) On the other hand, each attracting set shown in Figs. 9(b)–9(d) identically satisfies conditions $x = y$, $u = v$, and $z = w = 0$, although the solution emanating from a perturbed initial condition may go to the in-phase-locked periodic attracting set. We call it a P_2-invariant periodic chaotic attracting set.

2. Collapse of in-phase-locked periodic attracting set

Now let us consider itinerant behavior of attractors by increasing the parameter value of k_r from the value 0.877 70. We can observe a P_2-invariant periodic attracting set in T_2 with up to, e.g., $k_r = 0.877\,90$. On the other hand, the in-phase-locked periodic attracting set disappears at $k_r = 0.877\,75$ due to a boundary connection. Figure 10 shows the time series of the chaotic attractor by T_2^4. The phase portrait of the same attractor observed in T_2 is shown in Fig. 11. We see that it moves around in a wider region in the state space. Each phase portrait shown in Fig. 12 represents the behavior of the same attractor in appropriate short-term intervals. Figures 12(a)–12(d) show motions that behave around the sets shown in Figs. 9(a)–9(d), respectively. Therefore, the subspaces among which the chaotic attractor is itinerant are four quasiattracting states.

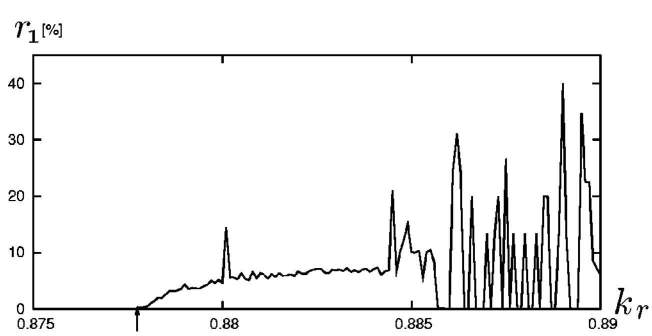

FIG. 15. The rate of counts r_1 for outputs around the stored pattern $\mathcal{P}^1$ and its reversed pattern during 32 768 iterations.

In Fig. 13 we show autocorrelation functions (ACF) for the chaotic time series x of Figs. 9 and 11. The ACF for four-periodic attracting sets (solid line) is almost zero; this means the chaotic attractor shown in Fig. 9 is similar to white noise. On the other hand, the ACF for the attractor showing chaotic itinerancy (dashed line) has some correlation, because it moves around four-periodic quasiattracting sets.

Here we consider the relation between itinerant behavior of internal states and itinerant memory dynamics of neuronal outputs that transit the two stored patterns. The output o_i of neuron i is given by $o_1=g(x+z)$, $o_2=g(u+w)$, $o_3=g(v-w)$, and $o_4=g(y-z)$, where g is the nonlinear function in Eq. (2). For the sake of simplicity, we now treat symbolic binary outputs 0 and 1, which are obtained by transforming the internal states through the Heaviside function. The set of symbolic outputs recalls one of the stored patterns $\mathcal{P}^1=(1,0,1,0)$ and $\mathcal{P}^2=(1,1,0,0)$, and their reversed patterns $\overline{\mathcal{P}^1}=(0,1,0,1)$ and $\overline{\mathcal{P}^2}=(0,0,1,1)$, if and only if the following conditions are satisfied: a pair of the symbolic outputs of o_i and o_j are in reverse phases, for $(i,j)=(1,4)$ and $(2,3)$.

Because P_2- and Q_2-invariant attracting sets are locked in-phase or satisfy $o_1=o_4$ and $o_2=o_3$ exactly, collapse of the invariant chaotic attracting sets is necessary for recalling any of the stored and reversed memory patterns. Indeed, as seen from Fig. 7, after merging of the invariant sets, the α branches rove over out-of-phase areas in the internal state space. To demonstrate the transition of memory states, Fig. 14 shows a time course of the Hamming distances between the output pattern at the discrete time t and each stored pattern, which is defined by $d_k(t)=\Sigma_{i=1}^4|o_i(t)-\mathcal{P}^k|$, for $k=1,2$. The values 0 and 4 of d_k correspond to the exact recall of the stored pattern $\mathcal{P}^k$ and its reversed pattern $\overline{\mathcal{P}^k}$, respectively, for $k=1,2$. The rate of counts r_1 that the output state satisfies the condition either $d_1<0.1$ or $d_1>3.9$ is shown in Fig. 15. Since the rate r_1 becomes a nonzero value at $k_r=0.877\,75$ when increasing k_r, the simultaneous occurrence of the collapse of in-phase-locked chaos and the generation of itinerant memory dynamics is numerically verified.

V. CONCLUDING REMARKS

We have investigated chaotic itinerancy observed in the chaotic neural network model described by the six-dimensional discrete dynamical system T_2. The behavior restricted to the Q_2-invariant subspace was investigated by analysis of the reduced subsystem T_1. The scenario for the generation of chaotic itinerancy observed in T_1 by increasing the parameter value of k_r is summarized as follows: first, successive period-doubling bifurcations occur and periodic points ${}_2D^m$ are generated, where $m=2^k$ $(k=0,1,\ldots,\infty)$; second, intersection of α-branches $W^+({}_2D^m)$ and $P(W^+({}_2D^m))$ $(m=2^k(k=\infty,\ldots,3,2))$ gives birth to in-phase-locked chaos as a periodic attracting set; and finally, intersection of α-branches $W^+({}_2D^4)$ and $W^+(T^n({}_2D^4))$ $(n=1,2,3)$ occurs and in-phase-locked chaos as a four-periodic attracting set collapses.

Itinerant memory dynamics in T_2 can be simultaneously observed when the collapse of the in-phase-locked chaos in T_1 occurs. Namely, in T_2, we have a chaotic behavior itinerating around both the periodic P_2-invariant attracting set and the periodic in-phase-locked attracting set, due to the boundary connection of the Q_2-invariant attracting set.

Significant characteristics of our model are that the dynamics of the subsystem T_1 is essential for the occurrence of chaotic itinerancy in T_2, and connection between two subsystems is also important for representing associative memory dynamics during the phenomenon of chaotic itinerancy. We consider that the six-dimensional system T_2 as a perturbation system from a direct sum of two identical subsystems T_1 is one of the smallest discrete dynamical system representing itinerant memory dynamics. Although the parameter $\sigma_k=1\mp d$ $(k=1,2)$ with a small value of d in the definition of the connection matrix is introduced to have different weights among stored patterns, the parameter plays an important role for constructing the slightly perturbed system or avoiding no interaction between two subsystems.

Due to symmetric properties of the system, behavior restricted to an invariant subspace can be investigated by analysis of a reduced subsystem. The setting of symmetry makes it easier for theoretical and numerical analysis. It should also be noted, however, that similar phenomena including chaotic itinerancy can be observed in a class of asymmetric systems affected by a parameter perturbation from the symmetric system, and all methods of analysis used in this paper are applicable to a general asymmetric system.

We have proposed a computational method to calculate the intersection of α branches of periodic points, and then the occurrence in our system has been illustrated. The manifold of the set satisfying the intersecting condition is locally codimension-one in the parameter space. Investigation of the global structure in a parameter space is an interesting future problem.

ACKNOWLEDGMENTS

This study is partially supported by the Advanced and Innovational Research program in Life Sciences and by Superrobust Computation Project in 21st Century COE Program on Information Science and Technology Strategic Core from the Ministry of Education, Culture, Sports, Science, and Technology, the Japanese Government.

[1] K. Aihara, "Chaotic neural networks," in *Bifurcation Phenomena in Nonlinear Systems and Theory of Dynamical Systems*, edited by H. Kawakami (World Scientific, Singapore, 1989), pp. 143–161.
[2] K. Aihara, T. Takabe, and M. Toyoda, "Chaotic neural networks," Phys. Lett. A **144**, 333–340 (1990).
[3] K. Aihara, "Chaos engineering and its application to parallel distributed processing with chaotic neural networks," Proc. IEEE **90**, 919–930 (2002).
[4] M. Adachi and K. Aihara, "Associative dynamics in a chaotic neural network," Neural Networks **10**, 83–98 (1997).
[5] T. Yoshinaga and H. Kawakami, "Chaotic wandering and bifurcations in coupled chaotic neurons," Nonlinear Anal. Theory, Methods Appl. **47**, 5357–5365 (2001).
[6] M. Komuro and K. Aihara, "Hierarchical structure among invariant subspaces of chaotic neural networks," Jpn. J. Indust. Appl. Math. **18**, 335–357 (2001).
[7] L. Chen and K. Aihara, "Chaotic simulated annealing by a neural network model with transient chaos," Neural Networks **8**, 915–930 (1995).
[8] L. Chen and K. Aihara, "Global searching ability of chaotic neural net-

works,'' IEEE Trans. Circuits Syst., I: Fundam. Theory Appl. **46**, 974–993 (1999).

[9] I. Tokuda, T. Nagashima, and K. Aihara, ''Global bifurcation structure of chaotic neural networks and its application to traveling salesman problems,'' Neural Networks **10**, 1673–1690 (1997).

[10] M. Hasegawa, T. Ikeguchi, and K. Aihara, ''Solving large scale traveling salesman problems by chaotic neurodynamics,'' Neural Networks **15**, 271–283 (2002).

[11] J. Matsuoka, Y. Sekine, K. Saeki, and K. Aihara, ''Analog hardware implementation of a mathematical model of an asynchronous chaotic neuron,'' IEICE Trans. Fundamentals **E85-A**, 389–394 (2002).

[12] Y. Horio, K. Aihara, and O. Yamamoto, ''Neuron-synapse IC chip-set for large-scale chaotic neural networks,'' IEEE Trans. Neural Networks (in press).

[13] C. Mira, *Chaotic Dynamics* (World Scientific, Singapore, 1987).

[14] G. Millerioux and C. Mira, ''Homoclinic and heteroclinic situations specific to two-dimensional noninvertible maps,'' Int. J. Bifurcation Chaos Appl. Sci. Eng. **7**, 39–70 (1997).

[15] E. R. Caianiello, ''Outline of a theory of thought-processes and thinking machines,'' J. Theor. Biol. **2**, 204–235 (1961).

[16] J. Nagumo and S. Sato, ''On a response characteristic of a mathematical neuron model,'' Kybernetik **10**, 155–164 (1972).

[17] H. Nozawa, ''A neural network model as a globally coupled map and applications based on chaos,'' Chaos **2**, 377–386 (1992).

[18] K. Kaneko and I. Tsuda, *Complex Systems: Chaos and Beyond* (Springer, Berlin, 2000).

[19] C. Mira, D. Fournier-Prunaret, L. Gardini, H. Kawakami, and J. C. Cathala, ''Basin bifurcations of two-dimensional noninvertible maps: Fractalization of basins,'' Int. J. Bifurcation Chaos Appl. Sci. Eng. **4**, 343–381 (1994).

[20] H. Kawakami, ''Algorithme numérique définisssant la bifurcation d'un point homocline,'' C. R. Acad. Sc. Paris, Série I **293**, 401–403 (1981).

[21] H. Kawakami and J. Matsuo, ''Bifurcation of doubly asymptotic motions in nonlinear systems,'' IEICE Trans. Fundamentals **J65-A**, 647–654 (1982).

[22] K. Yagasaki, ''Numerical detection and continuation of homoclinic points and their bifurcations for maps and periodically forced systems,'' Int. J. Bifurcation Chaos Appl. Sci. Eng. **8**, 1617–1627 (1998).

[23] H. Kawakami, ''Bifurcation of periodic responses in forced dynamic nonlinear circuits: computation of bifurcation values of the system parameters,'' IEEE Trans. Circuits Syst. **CAS-31**, 246–260 (1984).

[24] T. Yoshinaga, H. Kitajima, H. Kawakami, and C. Mira, ''A method to calculate homoclinic points of a two-dimensional noninvertible map,'' IEICE Trans. Fundamentals **E80-A**, 1560–1566 (1997).